Thermomechanical properties of confined fluids exposed to a shear strain

2000 J. Phys.: Condens. Matter 12 1545

(http://iopscience.iop.org/0953-8984/12/8/301)

J. Phys.: Condens. Matter **12** (2000) 1545–1568. Printed in the UK PII: S0953-8984(00)09539-4

Thermomechanical properties of confined fluids exposed to a shear strain

Henry Bock and Martin Schoen†

Institut für Theoretische Physik, Technische Universität Berlin, Hardenbergstraße 36, D-10623 Berlin, Germany

E-mail: henry@ozon.physik.tu-berlin.de and m.schoen@physik.tu-berlin.de

Received 15 November 1999

Abstract. The properties of a molecularly thin film of spherically symmetric molecules confined to a chemically heterogeneous slit-pore were investigated by Monte Carlo simulations in a grand mixed stress–strain ensemble. The slit-pore comprises two identical plane-parallel solid substrates, each of which consists of alternating strips of solid of two types: strongly adsorbing (width d_s) and weakly adsorbing. Under favourable thermodynamic conditions the confined film consists of fluid bridges—that is, a high(er)-density fluid over the strongly attractive strip surrounded by a low(er)-density fluid supported by the (outer) weakly attractive strips. By misaligning the opposite substrates, bridge phases can be exposed to a shear strain αs_x ($0 \leqslant \alpha \leqslant \frac{1}{2}$, s_x the side length of the simulation cell) and the associated shear stress T_{zx} of (fluidic) bridge phases can be calculated from molecular expressions. The stress curve $T_{zx}(\alpha s_x)$ is qualitatively similar to the one characteristic of solidlike films confined between atomically structured substrates in that the initial response to small shear strains is Hookean, and this is followed by an increasingly nonlinear regime up to the yield point where $T_{zx}(\alpha s_x)$ assumes its maximum. We also investigated the influence of chemical corrugation $c_r := d_s/s_x$ on $T_{zx}(\alpha s_x)$. With increasing c_r, yield strain and stress increase at first up to a maximum and decline thereafter. By employing the theory of corresponding states, $T_{zx}(\alpha s_x)$ is renormalized by yield stress and strain such that the results can be represented uniquely by a master curve independent of any system-dependent parameters.

1. Introduction

A key feature distinguishing bulk fluids (i.e., gases and liquids) from solids is the inability of the former to resist shear deformations. A bulk solid, on the other hand, responds to such a deformation similarly to a Hookean spring if the deformation is small enough—that is, the shear stress increases linearly with its conjugate strain. For larger shear strains the response of the solid becomes increasingly nonlinear and, as a result, the solid may eventually melt. Bulk shear melting is a typical first-order phase transition characterized by release of latent heat. Hookean behaviour at small shear strains followed by an increasingly nonlinear response to larger strains is also observed if a thin solidlike film is confined to spaces of molecular dimension(s) by solid substrates, a situation currently receiving a lot of attention both theoretically and experimentally (see [1] for an excellent review of experimental and theoretical work devoted to the rheology of molecularly thin confined films).

Experimentally the rheology of molecularly thin confined films can be investigated with nearly molecular precision in the surface forces apparatus (SFA) [2]. In the SFA a thin film is confined between the surfaces of two macroscopic cylinders arranged such that their axes are at

† Author to whom any correspondence should be addressed.

right angles. The surface of each cylinder is covered by a thin mica sheet with a silver backing, which permits one to measure the separation between the surfaces by optical interferometry. Since the cylinder radii are macroscopic, their surfaces may be taken as parallel on a *molecular* length scale around the point of minimum distance. In addition, the surfaces are *locally* planar, since mica can be prepared with atomic smoothness over molecularly large areas. This set-up is immersed in a bulk reservoir of the same fluid of which the film consists. Thus, at thermodynamic equilibrium, temperature T and chemical potential μ are equal in the two subsystems (i.e., film and bulk reservoir). A confined film can be exposed to a shear strain by attaching a movable stage to the upper substrate (i.e., wall) via a spring characterized by its spring constant and moving this stage at some constant velocity, say, in a direction parallel to the film–wall interface. This is usually effected under constant load (i.e., constant pressure exerted in the direction normal to the substrate surfaces). Experimentally it is observed that the upper wall first 'sticks' to the film as one might say because the upper wall remains stationary. From the known spring constant and the measured elongation of the spring, the shear stress sustained by the film can be determined. Beyond a critical shear strain (i.e., at the so-called 'yield point' corresponding to the maximum shear stress sustained by the film) the shear stress declines abruptly and the upper wall 'slips' across the surface of the film. If the stage moves at a sufficiently low speed the walls eventually come to rest again until the critical shear stress is once again attained, so the stick–slip cycle repeats itself periodically.

A key issue still under discussion is whether or not the rheological behaviour of confined phases reflects confinement-induced solidification or not (see [3, 4] and references therein). For instance, Klein and Kumacheva carried out SFA experiments in which an octamethylcyclotetrasiloxane (OMCTS) film confined between mica surfaces is exposed to a shear strain [3,4]. In SFA experiments OMCTS plays a prominent rôle because of its approximately spherically symmetric molecular structure, so models based upon 'simple' fluids (i.e., fluids composed of molecules having only translational degrees of freedom) can be employed theoretically to understand many important aspects of SFA experiments [5] (see also below). In their work Klein and Kumacheva find that for large substrate separations of 1160 Å, 'confined' OMCTS behaves essentially like a bulk liquid. In this case a characteristic relative lateral displacement of the upper substrate is observed on account of thermal noise (see figure 6(a) in [3]). This motion remains unaltered if the distance between substrate surfaces is reduced down to approximately 62 Å. However, for a slightly smaller substrate separation of about 54 Å the lateral motion of the upper substrate suddenly disappears as if the film were capable of 'gluing' the substrate to some fixed position in space (see figures 6(b) and 6(c) of [3]). Klein and Kumacheva take the abrupt disappearance of lateral substrate motion as evidence of confinement-induced solidification of OMCTS in the narrow gaps between the mica surfaces. If the above films are exposed to oscillatory shear forces, only the thinnest one is capable of sustaining a shear stress, which Klein and Kumacheva take as further evidence for a liquid–solid phase transition in OMCTS films triggered by confinement.

Theoretically, most previous studies support the notion of confinement-induced solidification of 'simple'-fluid films between commensurately structured substrate surfaces [1]. These substrates are composed of individual atoms arranged according to some solid structure such that the lattice constant of the confined solidlike film, ℓ_{f}, and that of the substrate, ℓ, are identical. Solidification of the film (which is in thermodynamic equilibrium with bulk *liquid*) occurs by means of a template effect if the separation between the planar substrates is comparable to the range of the film–substrate interaction potential and if the substrates are aligned favourably in transverse directions. Thus, by gradually misaligning the substrates, a solidlike film can be exposed to a shear strain and the conjugate shear stress can be calculated.

The approaches used to study confined films under shear theoretically can generally be grouped into two different categories which may be labelled 'dynamical' [6–12] and 'quasi-static' [13–20]. In the dynamical approaches a stationary nonequilibrium state is created by either applying an external driving force [6] or by explicitly moving a substrate wall [7, 9–12] in nonequilibrium molecular dynamics (NEMD) simulations to mimic dynamical aspects of a corresponding SFA experiment directly on a molecular scale. However, the relationship between NEMD simulations [7, 9–12] and SFA experiments remains obscure for a number of reasons. First, to describe the motion of the substrate wall on a physical timescale, an equation of motion needs to be solved which inevitably involves the mass of the wall. However, there are no physical criteria on which the choice of a specific value for this mass could be based. Second, even though the wall is a macroscopic object in the SFA experiment, its mass cannot be too much larger than the mass of a film molecule in the NEMD simulations because otherwise the wall would remain at rest on the timescale on which film molecules move. In fact, the ratio of the mass of a single film molecule to that of the entire wall is sometimes as small as 1/8 [11, 12], so one can expect relaxation phenomena in the film to depend sensitively (and therefore unphysically from an experimental perspective) on this arbitrarily selected wall mass [21]. Third, the speed at which the walls are slid in the SFA experiment is typically of the order of 10^{-9}–10^{-7} Å ps^{-1} [22], so under realistic conditions the walls remain practically stationary on a typical length scale and timescale of molecular relaxation processes. In NEMD simulations of SFA models one is therefore ineluctably forced to resort to unrealistically high shear rates (even if one assumes the film to be composed of molecules much heavier than rare-gas atoms) to obtain a tractable signal-to-noise ratio for quantities of interest. Thus, the relevance of molecular-scale dynamical simulations to boundary lubrication phenomena remains highly questionable.

Surprisingly little attention has been paid so far to the fact that even a fluidlike confined film, if exposed to a shear strain, may exhibit features normally characteristic of a solid—that is, the strain dependence of the shear stress obeys Hooke's law initially; for larger strains a yield point exists even though the associated yield stress is reduced in magnitude compared with that for a solidlike film. For example, if ℓ is reduced slightly such that $\ell/\ell_f \lesssim 0.94$ (with ℓ_f referring to a bulk solid composed of the confined material having the same crystallographic structure as the substrate), a confined film is prevented from solidifying regardless of substrate alignment. This was demonstrated by Schoen *et al* who studied various translational and bond-orientational structural correlation functions for a 'simple'-fluid film confined between such incommensurate substrate surfaces (see figure 5 in [13]). However, the shear stress characteristic of the film still exhibits the Hookean regime for small deformations and a yield point at larger shear strains (see figure 2(b) in [13]). However, the yield stress is lower by about a factor of 3 compared with that of a corresponding solidlike film confined between commensurately structured ($\ell/\ell_f = 1$) substrates (see figure 2(b), figure 2(c) in [13]). The purpose of the present study is to provide further evidence for the irrelevance of solidlike structures as far as the qualitative response of confined matter to shear deformations is concerned. In fact, our results indicate that *any* sufficiently thin confined film will probably be capable of sustaining a shear strain provided that it is inhomogeneous in the direction of the applied strain regardless of its physical state.

The remainder of the paper is organized as follows. In section 2 we introduce our model system. Section 3 is devoted to a brief summary of the thermodynamics of strained confined films and to an introduction of molecular expressions for relevant thermomechanical properties. Results are presented in section 4. The paper ends in section 5 with a summary of our main findings and their discussion.

2. Model system

Our model consists of a film composed of spherically symmetric molecules sandwiched between the surfaces of two solid substrates. The substrate surfaces are planar, parallel, and separated by a distance s_z along the z-axis of the coordinate system. The substrates are semi-infinite in the z-direction, occupying the half spaces $s_z/2 \leqslant z \leqslant \infty$ and $-\infty \leqslant z \leqslant -s_z/2$, and are infinite in the x- and y-directions. Each substrate comprises alternating slabs of two types: strongly adsorbing and weakly adsorbing. The 'strong' and 'weak' slabs have widths d_s and $d_w/2$, respectively, in the x-direction and are infinite in the y-direction. If the substrates are aligned as in figure 1 the system is thus periodic in the x-direction with period d_s+d_w and its properties are translationally invariant in the y-direction. In practice we take the system to be a finite piece of the film, imposing periodic boundary conditions [23] on the planes $x = \pm s_x/2$ and $y = \pm s_y/2$ where s_α ($\alpha = x, y$) is the side length of the system in the α-direction.

Substrate atoms are assumed to be of the same 'diameter' (σ) and to occupy the sites of the face-centred cubic (fcc) lattice (the substrate surfaces are taken to be (100) planes) where ℓ is taken to be the same for the atomic species in both strong and weak slabs. Thus, substrate atoms forming these slabs are distinguished only by their respective strengths of interaction with film molecules. We assume the total potential energy to be a sum of pairwise-additive Lennard-Jones (LJ) (12, 6)-type potentials $u(r)$ (see section 4). For the interaction between a pair of film molecules the potential-well depth $\epsilon = \epsilon_{ff}$ (i.e., $u_{ff}(r)$). The nanoscale heterogeneity of the substrate is characterized by $\epsilon = \epsilon_{fs}$ (i.e., $u_{fs}(r)$) for the interaction of a fluid molecule with a substrate atom in the strong (central) slab, and by $\epsilon = \epsilon_{fw}$ (i.e., $u_{fw}(r)$) for the interaction of a fluid molecule with a substrate atom in either of the two weak (outer) slabs (see figure 1). We take $\epsilon_{fs}/\epsilon_{ff} = 1.25$ and $\epsilon_{fw}/\epsilon_{ff} = 10^{-3}$.

Since we are concerned with the effects of nanoscale chemical heterogeneity on the behaviour of a confined fluid, we expect details of the substrate structure at the atomic level not to matter greatly. Therefore, we adopt a mean-field representation of the interaction of a fluid molecule with the substrate, which we obtain by averaging the fluid–substrate interaction potential over positions of substrate atoms in the x–y plane. The resulting mean-field potential can be expressed as [24–26]

$$\begin{aligned}\Phi^{[k]} = -3\pi\left(\frac{\sigma}{\ell}\right)^2 \sum_{m=-\infty}^{\infty}\sum_{m'=0}^{\infty}\Bigg\{&(\epsilon_{fw}-\epsilon_{fs})\Bigg[\Delta\left(\widetilde{x}+\frac{d_s}{2}-ms_x,\ \frac{s_z}{2}+m'\delta_\ell \pm z\right)\\ &-\Delta\left(\widetilde{x}-\frac{d_s}{2}-ms_x,\ \frac{s_z}{2}+m'\delta_\ell \pm z\right)\Bigg]\\ &-\epsilon_{fw}\Bigg[\Delta\left(\widetilde{x}+\frac{s_x}{2}-ms_x,\ \frac{s_z}{2}+m'\delta_\ell \pm z\right)\\ &-\Delta\left(\widetilde{x}-\frac{s_x}{2}-ms_x,\ \frac{s_z}{2}+m'\delta_\ell \pm z\right)\Bigg]\Bigg\}\end{aligned} \tag{1}$$

where δ_ℓ is the spacing between successive crystallographic planes in the $\pm z$-direction. The sign is chosen according to the convention $+ \leftrightarrow k = 1$ and $- \leftrightarrow k = 2$.

Because of the chemical corrugation of each substrate (i.e., the presence of strongly and weakly adsorbing slabs), a confined fluid can be exposed to a shear strain by misaligning the substrates in the x-direction according to

$$\widetilde{x} := \begin{cases} x & k = 1 \\ x - \alpha s_x & k = 2 \end{cases} \tag{2}$$

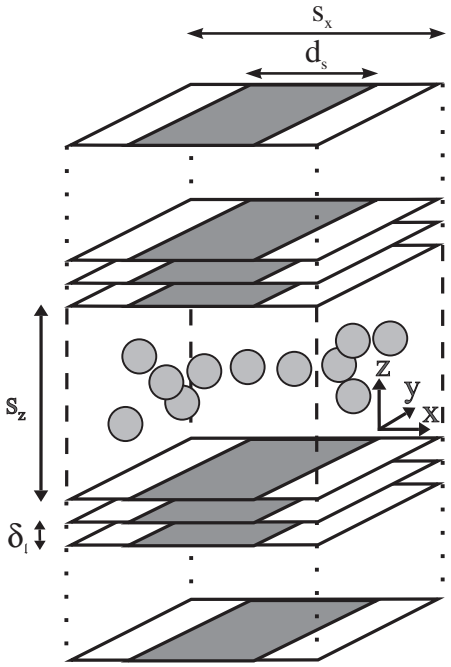

Figure 1. A schematic diagram of a simple fluid confined by a chemically heterogeneous model pore. Fluid molecules (grey spheres) are spherically symmetric. Each substrate consists of a sequence of crystallographic planes separated by a distance δ_ℓ along the z-axis. The surface planes of the two opposite substrates are separated by a distance s_z. Periodic boundary conditions are applied in the x- and y-directions (see the text).

where $\alpha := \delta_\alpha / s_x$ is a dimensionless number and δ_α is the magnitude of the relative displacement of the substrates with respect to each other in the $+x$-direction. According to this definition and because of the periodicity of the substrate structure $\{\alpha | 0 \leqslant \alpha \leqslant \frac{1}{2}\}$, $\alpha = 0$ refers to perfectly aligned substrates (i.e., substrates 'in registry') whereas $\alpha = \frac{1}{2}$ is the maximum misalignment (i.e., substrates 'out of registry'). In (1) the auxiliary function Δ is defined as (see [26] for details)

$$\Delta(x'', z'') := \frac{21}{32} I_3(x'', z'') - I_4(x'', z'') \tag{3}$$

where

$$I_3(x'', z'') = \frac{x'' \sigma^{10}}{9 z''^2 \sqrt{R^9}} \left[1 + \frac{8}{7} S + \frac{48}{35} S^2 + \frac{64}{35} S^3 + \frac{128}{35} S^4 \right] \tag{4}$$

$$I_4(x'', z'') = \frac{x'' \sigma^4}{3 z''^2 \sqrt{R^3}} [1 + 2S] . \tag{5}$$

Here $R := x''^2 + z''^2$ and $S := R / x''^2$.

It is important at this point to appreciate the symmetry of the *whole* fluid–substrate potential $\Phi = \Phi^{[1]} + \Phi^{[2]}$. When the z-coordinate of the film is reflected through the mirror plane $z = 0$, $-z$ in the arguments $z'' = s_z/2 + m' \delta_\ell \pm z$ of $\Phi^{[1]}$ changes to $+z$ in the arguments of $\Phi^{[2]}$ and vice versa. The sum Φ is therefore invariant under reflections in the $z = 0$ plane. Likewise, $\Phi^{[1]}$ and $\Phi^{[2]}$ are separately invariant under reflection in the x-plane, although the proof involves

more subtle interconversions. For example, under the transformation $\widetilde{x} \to -\widetilde{x}$,

$$\Delta\left(\widetilde{x} + \frac{d_s}{2} - ms_x, z''\right) \overset{\widetilde{x}\to-\widetilde{x}}{\longrightarrow} \Delta\left(-\widetilde{x} + \frac{d_s}{2} - ms_x, z''\right) = -\Delta\left(\widetilde{x} - \frac{d_s}{2} + ms_x, z''\right) \tag{6}$$

where the equality holds because both I_3 and I_4 are odd functions of x''. Likewise the second term ($m \geqslant 0$) is converted into the negative first term ($m \leqslant 0$), so the transformation $\widetilde{x} \to -\widetilde{x}$ interchanges the first and second terms in (1) with the appropriate change in sign. The same applies to the third and fourth terms in (1) as one can easily verify. Therefore, and because $\{m|-\infty \leqslant m \leqslant \infty\}$ in (1), $\Phi^{[k]}$ is an even function of $\widetilde{x}$.

Because of this symmetry, $\Phi^{[k]}$ need only be represented in one half (say, $0 \leqslant x \leqslant s_x/2$, $-s_z/2 \leqslant z \leqslant s_z/2$) of the x–z plane [26]. In this half, $\Phi^{[k]}$ is computed at the nodes of a two-dimensional grid prior to the simulation where we employ a mesh of $\delta_x = \delta_z = 1.25 \times 10^{-2}\sigma$. In practice, a sufficiently accurate numerical representation of $\Phi^{[k]}$ is obtained by limiting m and m' in (1) to the respective ranges $\{m|-2 \leqslant m \leqslant 2\}$ and $\{m'|0 \leqslant m' \leqslant 50\}$ as tests in [26] revealed. During the simulation the value of $\Phi^{[k]}$ corresponding to the actual position of a fluid molecule is computed by two-dimensional interpolation between the nodes, as detailed in [26].

3. Thermomechanical properties

3.1. Thermodynamic considerations.

Henceforth we wish to investigate confined films exposed to shear strains under conditions closely resembling those of parallel SFA experiments. Therefore, we perceive the confined film as an open system in the thermodynamic sense. The film is furthermore subjected to a fixed compressional stress T_{zz} (i.e., load) in the direction normal to the substrate plane. By a treatment parallel to the one detailed in section II.A.2 of [5] one can show that under these conditions the generalized Gibbs potential

$$\widehat{\mathcal{G}} := \mathcal{U} - T\mathcal{S} - N\mu - T_{zz}s_x s_y s_z \tag{7}$$

is minimum in thermodynamic equilibrium. In (7), $\mathcal{U}$ is the internal energy, $\mathcal{S}$ is the entropy, and N is the number of fluid molecules. With the aid of Gibbs' fundamental equation

$$\mathrm{d}\mathcal{U} = T\ \mathrm{d}\mathcal{S} + \mu\ \mathrm{d}N + T_{xx}s_y s_z\ \mathrm{d}s_x + T_{yy}s_x s_z\ \mathrm{d}s_y + T_{zz}s_x s_y\ \mathrm{d}s_z + T_{zx}s_x s_y\ \mathrm{d}(\alpha s_x) \tag{8}$$

the exact differential of $\widehat{\mathcal{G}}$ can be cast as

$$\begin{aligned}\mathrm{d}\widehat{\mathcal{G}} = {} & -\mathcal{S}\ \mathrm{d}T - N\ \mathrm{d}\mu + (T_{xx} - T_{zz})s_z s_y\ \mathrm{d}s_x + (T_{yy} - T_{zz})s_z s_x\ \mathrm{d}s_y \\ & - As_z\ \mathrm{d}T_{zz} + T_{zx}A\ \mathrm{d}(\alpha s_x)\end{aligned} \tag{9}$$

where $A := s_x s_y$ is the fluid–substrate interfacial area, $T_{\beta\beta}$ is the compressional stress exerted on a plane pointing in the β-direction ($\beta = x, y, z$), and T_{zx} is the shear stress conjugate to the shear strain αs_x. Thus, $\{T, \mu, s_x, s_y, T_{zz}, \alpha s_x\}$ is the set of natural variables of $\widehat{\mathcal{G}}$ [5]. Because of the symmetry of the confined fluid (see figure 1) it is furthermore clear that

$$\zeta(T, \mu, s_x, T_{zz}, \alpha s_x) := (T_{yy} - T_{zz})s_z \tag{10}$$

is independent of s_y, so for fixed T, μ, s_x, T_{zz}, and αs_x, $\widehat{\mathcal{G}}$ is a homogeneous function of degree one in s_y. Hence, under these constraints Euler's theorem applies and one obtains

$$\widehat{\mathcal{G}} = \zeta A \qquad \text{fixed } T, \mu, s_x, T_{zz}, \alpha s_x \tag{11}$$

where we take the zero of $\widehat{\mathcal{G}}$ to coincide with $s_y = 0$. Because of (11), ζ can be interpreted as an areal free-energy density (i.e., a free energy per unit area).

3.2. Molecular expressions for the shear stress

By means of a quantum-statistical treatment one can furthermore show that [5]

$$\widehat{\mathcal{G}} = -\beta^{-1} \ln \chi \tag{12}$$

where $\beta := 1/(k_B T)$ (k_B: Boltzmann's constant) and $\chi(T, \mu, s_x, s_y, T_{zz}, \alpha s_x)$ is the partition function in the present grand mixed stress–strain ensemble. In the classical limit (with which we shall be exclusively concerned) one can show [5] that

$$\chi(T, \mu, s_x, s_y, T_{zz}, \alpha s_x) = \sum_N \exp(\beta\mu N) \sum_{s_z} \exp(\beta T_{zz} A s_z) Q(N, T, s_x, s_y, s_z, \alpha s_x) \tag{13}$$

where

$$Q = \frac{Z}{N! \Lambda^{3N}} \tag{14}$$

is the canonical ensemble partition function after the usual analytical integration over momentum space and

$$\Lambda = \sqrt{h^2 \beta / 2\pi m}$$

(h: Planck's constant; m: molecular mass) is the thermal de Broglie wavelength. In (14),

$$Z = \prod_{i=1}^{N} \int_V \mathrm{d}\boldsymbol{r}_i \, \exp[-\beta U(\boldsymbol{r}^N)] \tag{15}$$

where the N-particle configuration $\boldsymbol{r}^N$ is represented by the $3N$-dimensional vector $(\boldsymbol{r}_1, \boldsymbol{r}_2, \ldots, \boldsymbol{r}_N)$. For the present system the configurational energy U can be cast as

$$U(\boldsymbol{r}^N) = \frac{1}{2} \sum_{i=1}^{N} \sum_{j=1 \neq i}^{N} u_{\mathrm{ff}}(r_{ij}) + \sum_{k=1}^{2} \sum_{i=1}^{N} \Phi^{[k]}(\widetilde{x}_i, z_i; d_s, s_x, s_z) =: U_{\mathrm{FF}} + \sum_{k=1}^{2} U_{\mathrm{FS}}^{[k]}. \tag{16}$$

Following the procedure detailed in [27], it is easy to show from (9)–(16) that

$$\begin{aligned} A T_{zx} &= \left(\frac{\partial \widehat{\mathcal{G}}}{\partial(\alpha s_x)} \right)_{T, \mu, s_x, s_y, T_{zz}} \\ &= -\frac{k_B T}{N! \Lambda^{3N} \chi} \sum_N \exp(\beta\mu N) \sum_{s_z} \exp(\beta T_{zz} A s_z) \left(\frac{\partial Z}{\partial(\alpha s_x)} \right)_{T, s_x, s_y} \\ &= \left\langle \frac{\partial U_{\mathrm{FS}}^{[2]}}{\partial(\alpha s_x)} \right\rangle = -\left\langle \sum_{i=1}^{N} f_x^{[2]}(\widetilde{x}_i, z_i) \right\rangle = -\left\langle F_x^{[2]} \right\rangle \end{aligned} \tag{17}$$

where

$$f_x^{[k]}(\widetilde{x}_i, z_i; d_s, s_x, s_z) := -\frac{\partial \Phi^{[k]}(\widetilde{x}_i, z_i; d_s, s_x, s_z)}{\partial x_i} \tag{18}$$

is the x-component of the force exerted *by* the upper substrate ($k = 2$) *on* film molecule i and $F_x^{[2]}$ is the total force exerted by the upper substrate on a particular configuration of film molecules. As was shown in [26], the expression for $f_x^{[k]}$ matches (1) formally except for the function $\Delta(x'', z'')$ which must be replaced by

$$\Gamma(x'', z'') := \frac{21}{32} I_1(x'', z'') - I_2(x'', z'') \tag{19}$$

where

$$I_1(x'', z'') := \sqrt{\left(\frac{\sigma^2}{R} \right)^{11}} \tag{20}$$

and

$$I_2(x'', z'') := \sqrt{\left(\frac{\sigma^2}{R}\right)^5}. \tag{21}$$

Because of (18) we term (17) the 'force expression' for T_{zx}. Mechanical stability requires

$$\left\langle F_x^{[1]} \right\rangle + \left\langle F_x^{[2]} \right\rangle = 0 \tag{22}$$

thus providing a useful check on internal consistency of the computer simulation results (see table 1).

Table 1. Comparison of virial and force expressions for T_{zx}. Entries are obtained from Monte Carlo simulations in the grand mixed stress–strain ensemble for various sheared bridge-phase morphologies (characterized by $\langle s_z \rangle$).

			From (17)		From (24)
c_r	αs_x	$\langle s_z \rangle$	$\langle F_x^{[1]} \rangle / A$	$\langle F_x^{[2]} \rangle / A$	T_{zx}
$\frac{2}{10}$	1.70	2.122	0.068	−0.068	0.068
$\frac{4}{10}$	1.75	2.069	0.144	−0.144	0.144
$\frac{4}{10}$	2.50	2.075	0.160	−0.161	0.160
$\frac{4}{10}$	1.75	3.060	0.086	−0.086	0.087
$\frac{4}{10}$	2.50	3.067	0.101	−0.101	0.101
$\frac{4}{10}$	1.75	3.989	0.051	−0.051	0.049
$\frac{4}{10}$	2.25	3.974	0.059	−0.058	0.059
$\frac{4}{10}$	2.50	4.013	0.060	−0.058	0.056
$\frac{6}{10}$	1.75	2.063	0.141	−0.143	0.142
$\frac{6}{10}$	2.50	2.064	0.157	−0.153	0.154
$\frac{6}{10}$	1.75	3.038	0.084	−0.084	0.084
$\frac{6}{10}$	2.50	3.042	0.092	−0.093	0.093
$\frac{8}{10}$	1.75	2.054	0.066	−0.064	0.065
$\frac{8}{10}$	2.50	2.056	0.034	−0.034	0.034

Notice, however, that

$$f_x^{[k]} \overset{\widetilde{x} \to -\widetilde{x}}{\longrightarrow} -f_x^{[k]} \tag{23}$$

indicating that $f_x^{[k]}$ is an odd function of $\widetilde{x}$ which follows from the same considerations as were applied to $\Phi^{[k]}$ in section 2. The odd symmetry of $f_x^{[k]}$ under transformations $\widetilde{x} \to -\widetilde{x}$ is a direct consequence of the symmetry of I_1 and I_2 which (unlike their counterparts I_3 and I_4, see (4), (5)) are even functions of x''. For $\alpha = 0, \frac{1}{2}$, the probability density distribution in the grand mixed stress–strain ensemble is symmetric with respect to the plane $x = 0$ with the result that, because of the symmetry of $f_x^{[k]}$, $\langle F_x^{[k]} \rangle \equiv 0$. Notice, however, that the probability density distribution is not symmetric with respect to the plane $x = 0$ for $\{\alpha | 0 < \alpha < \frac{1}{2}\}$. Consequently, one expects nonvanishing shear stresses over this range of shear strains.

In [27] it was also demonstrated that an alternative expression

$$T_{zx} = T_{zx}^{\mathrm{FF}} + T_{zx}^{\mathrm{FS}} \tag{24}$$

can be derived for the shear stress in the spirit of Hill [28]. This treatment, fully detailed in [27], starts from the explicit expression

$$Z = \prod_{i=1}^{N} \int_{-s_y/2}^{s_y/2} \mathrm{d}y_i \int_{-s_z/2}^{s_z/2} \mathrm{d}z_i \int_{-s_x/2+\alpha s_x(2z_i+s_z)/2s_z}^{s_x/2+\alpha s_x(2z_i+s_z)/2s_z} \mathrm{d}x_i \, \exp[-\beta U(\boldsymbol{r}^N)] \tag{25}$$

for the partition function (see (15)) of a fluid in slit geometry confined by substrates that are misaligned in the x-direction according to (2). Introducing the transformation

$$x_i \to x_i' = x_i - \alpha s_x(2z_i + s_z)/2s_z$$

it is easy to verify that the integration limits in (25) become independent of the shear strain. It is then straightforward to evaluate the partial derivative $\partial Z/\partial(\alpha s_x)$ in (17) employing Leibniz's rule for the differentiation of a parameter integral [29]. After reversing the coordinate transformation one eventually obtains (24) where the fluid–fluid (FF) contribution is given by

$$T_{zx}^{\mathrm{FF}} = \frac{1}{2A}\left\langle \frac{1}{s_z} \sum_{i=1}^{N} \sum_{j=1\neq i}^{N} u_{\mathrm{ff}}'(r_{ij}) \frac{x_{ij} z_{ij}}{r_{ij}} \right\rangle \tag{26}$$

and $u_{\mathrm{ff}}'(r) := \mathrm{d}u_{\mathrm{ff}}(r)/\mathrm{d}r$. By similar arguments (see [27] for details) one can derive

$$T_{zx}^{\mathrm{FS}} = -\frac{1}{A}\left\langle \frac{1}{s_z} \sum_{k=1}^{2} \sum_{i=1}^{N} f_{x,i}^{[k]}\left(z_i \pm \frac{s_z}{2}\right) \right\rangle \tag{27}$$

assuming that the origin of the coordinate system coincides with the fixed (average) position of the centre of mass of the confined fluid. Equation (24) is termed the 'virial expression' for T_{zx}. Both force and virial routes to T_{zx} are useful for checking the reliability of the simulations. As can be seen from table 1, the agreement between the two expressions is very good even though T_{zx} is rather small under typical conditions of this work. By the same approach one can derive

$$T_{yy} \equiv T_{yy}^{\mathrm{FF}} = -\frac{k_{\mathrm{B}}T}{A}\left\langle \frac{N}{s_z} \right\rangle + \frac{1}{2A}\left\langle \frac{1}{s_z} \sum_{i=1}^{N} \sum_{j=1\neq i}^{N} u_{\mathrm{ff}}'(r_{ij}) \frac{y_{ij} y_{ij}}{r_{ij}} \right\rangle \tag{28}$$

where, however, $T_{yy}^{\mathrm{FS}} \equiv 0$ because the fluid–substrate potential is translationally invariant in the y-direction.

Another quantity of interest in the context of this work is the shear modulus

$$c_{44} := \left(\frac{\partial^2 \widehat{\mathcal{G}}}{\partial(\alpha s_x)^2}\right)_{T,\mu,s_x,s_y,T_{zz}} = \left(\frac{\partial T_{zx}}{\partial(\alpha s_x)}\right)_{T,\mu,s_x,s_y,T_{zz}} \tag{29}$$

in Voigt's notation [30]. By a tedious but straightforward calculation parallel to the one detailed in [14], one can show from (13)–(17) and (29) that

$$Ac_{44} = -\beta\left[\left\langle F_x^{[2]2}\right\rangle - \left\langle F_x^{[2]}\right\rangle^2\right] + \left\langle \frac{\partial^2 U_{\mathrm{FS}}^{[2]}}{\partial(\alpha s_x)^2} \right\rangle. \tag{30}$$

From (17), and (30) it is clear that

$$\frac{\partial^2 U_{\mathrm{FS}}^{[2]}}{\partial(\alpha s_x)^2} = -\frac{\partial F_x^{[2]}}{\partial(\alpha s_x)} = -\sum_{i=1}^{N} \frac{\partial f_x^{[2]}(\widetilde{x}_i, z_i)}{\partial(\alpha s_x)}. \tag{31}$$

The expression for the partial derivative of $f_x^{[k]}$ is identical in form with (1) except that $\Delta(x'', z'')$ has to be replaced by (see (20), (21))

$$\Theta(x'', z'') := -\frac{x''}{R}(11I_1 - 5I_2) \tag{32}$$

which (like $\Delta(x'', z'')$ in (1)) is an odd function of x''. Thus, from the same symmetry considerations as were applied to $f_x^{[k]}$ above and to $\Phi^{[k]}$ in section 2 it follows that $c_{44} \neq 0$ over the entire range of shear strains, i.e. for $\{\alpha | 0 \leqslant \alpha \leqslant \frac{1}{2} \vee \alpha \neq \alpha^{\mathrm{yd}}\}$ where α^{yd} refers to the yield strain (see section 4.1.1). Again for symmetry reasons (i.e., because of (22)), an alternative expression can be obtained, replacing, however, in (30), $U_{\mathrm{FS}}^{[2]}$ by $U_{\mathrm{FS}}^{[1]}$ and $F_x^{[2]}$ by $F_x^{[1]}$.

4. Results

Results were obtained for $T = 1.0$, $\mu = -11.455$ (assuming argon), and $T_{zz} = 0.0$ where all quantities are expressed in the customary dimensionless (i.e., 'reduced') units. That is, energy is expressed in units of ϵ_{ff}, length in units of σ, temperature in units of $\epsilon_{\mathrm{ff}}/k_{\mathrm{B}}$, and stress in units of $\sigma^3/\epsilon_{\mathrm{ff}}$.

Equilibrium properties of the confined film are obtained in Monte Carlo simulations in the grand mixed stress–strain ensemble introduced in section 3. However, instead of using in these simulations the 'full' Lennard-Jones (LJ) (12, 6) potential to describe the fluid–fluid interaction, we employ a 'shifted-force' version defined such that the LJ (12, 6) potential and its first derivative vanish at the cut-off radius $r_{\mathrm{c}} = 3.5$. Since $u_{\mathrm{ff}}(r_{\mathrm{c}}) \approx 0$ as far as the full LJ (12, 6) potential is concerned, the phase behaviour of a (bulk) fluid based upon the shifted-force potential differs only marginally from that of the full LJ (12, 6) fluid. However, as pointed out in [31], the shifted-force potential is advantageous because no long-range correction has to be applied to the fluid–fluid interaction; that is, u_{ff} vanishes by definition for all $\{r | r \geqslant r_{\mathrm{c}}\}$. This is particularly important in the present case where the Monte Carlo algorithm, fully described in [19], involves changes in the number of molecules because the thermodynamic state is specified by μ as one of the state variables. The associated density change of $\pm 1/N$ between pairs of consecutive trial configurations would require an analytic energy correction during the generation of the Markov chain as far as the full (i.e., infinitely long-range) LJ (12, 6) potential is concerned. While explicit expressions for correction terms are available for the present slit-pore geometry [32], their application is not unproblematic under all circumstances [33].

Under the present thermodynamic conditions, $\alpha = 0$, and $2.0 \leqslant d_{\mathrm{s}} \leqslant 8.0$, the confined fluid forms a 'bridge' phase; that is, a high(er)-density portion of the fluid is stabilized between the (aligned) strongly adsorbing strips whereas a low(er)-density regime exists over the two outer weakly adsorbing strips. This characteristic structure is illustrated by the plot of the local density $\rho(x, z)$ in figure 2(a). Bridge phases may coexist with liquidlike or gaslike phases characterized by high(er)- and low(er)-density fluids, respectively, supported by the entire substrate material (see figure 2(b), figure 2(c)). By virtue of its structure, only bridge phases can sustain a substantial shear strain. However, if a bridge phase is exposed to a sufficiently large shear strain it may undergo a first-order phase transition and form either a gaslike or a liquidlike phase [34, 35]. The phase behaviour of confined fluids involving gaslike, liquidlike, and bridge phases is extensively discussed in a number of papers both under shear [34, 35] and for substrates in registry [24, 36, 37]—that is, in the absence of a shear strain.

4.1. Stress curves

4.1.1. General features of stress curves. The key quantity calculated in the present Monte Carlo simulations is the stress curve $T_{zx}(\alpha s_x)$ accessible via (17)–(22) and the alternative expressions in (24)–(27). Regardless of the thermodynamic state and the thickness (i.e., s_z) of a bridge phase, a typical stress curve plotted in figure 3 exhibits the following features:

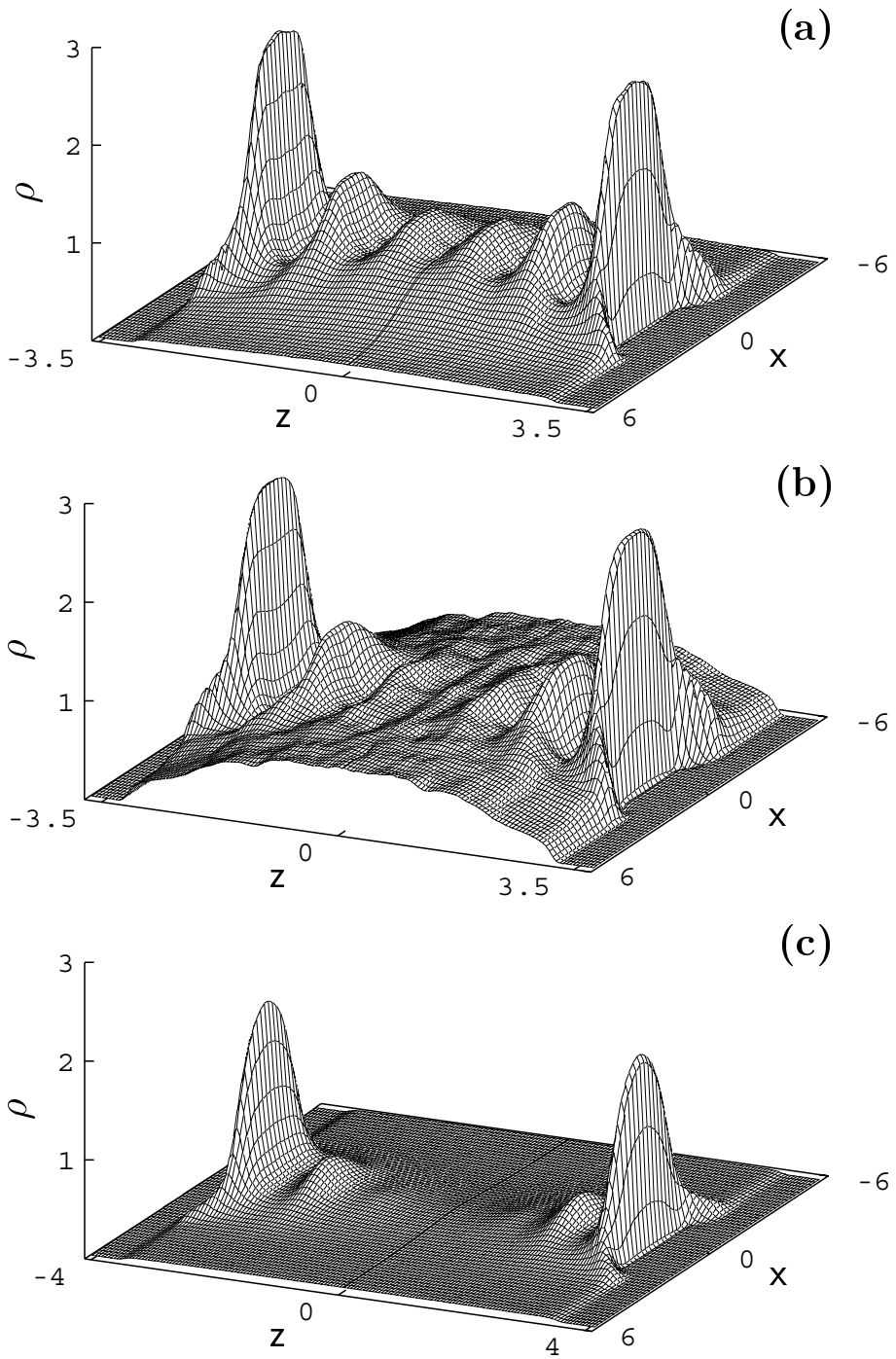

Figure 2. Typical microscopic structures of fluids confined between chemically striped substrates (see figure 1). The plots show local density $\rho(x, z)$ as a function of position in the x–z plane: (a) bridge phase ($s_z = 7.2$); (b) liquidlike phase ($s_z = 7.5$); (c) gaslike phase ($s_z = 8.2$) (see the text). Data are taken from [24] for a thermodynamic state specified by $T = 1.0$ and $\mu = -11.50$; the substrate parameters are $s_x = 12.0$, $d_s = 4.0$, $d_w = 8.0$ with ϵ_{fs} and ϵ_{fw} as in this work.

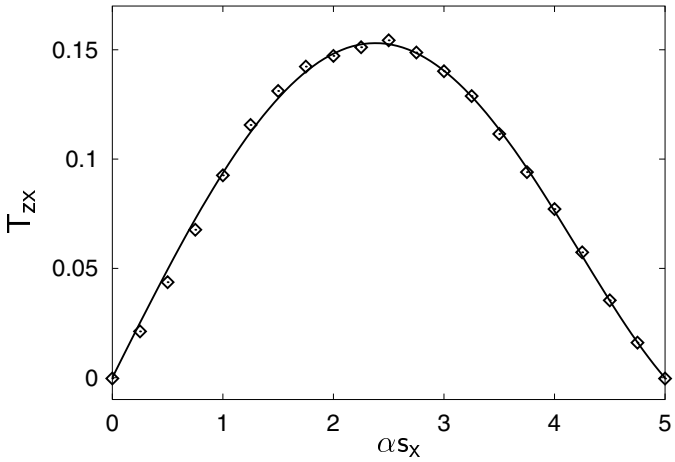

Figure 3. A typical stress curve $T_{zx}(\alpha s_x)$ for a monolayer bridge phase and $c_r = \frac{5}{10}$. The solid line is a least-squares fit of a polynomial to the (discrete) Monte Carlo data points (◇) intended to guide the eye.

(a) For vanishing shear strain (i.e., $\alpha = 0$), $T_{zx}(0) \equiv 0$ for symmetry reasons.
(b) $T_{zx}(\alpha s_x)$ depends linearly on the shear strain αs_x in the limit $\alpha \to 0$; that is, the response of the bridge phase to small shear strains follows Hooke's law.
(c) For larger shear strains, negative deviations from Hooke's law are observed, eventually leading to a yield point $(\alpha^{yd}, T_{zx}^{yd})$ defined by the constitutive equation

$$\left(\frac{\partial T_{zx}}{\partial(\alpha s_x)}\right)_{T,\mu,s_x,s_y,T_{zz}}\Bigg|_{\alpha=\alpha^{yd}} = 0 \tag{33}$$

or, alternatively (see (29)),

$$c_{44}(\alpha^{yd} s_x) = 0 \qquad \text{fixed } T,\ \mu,\ s_x,\ s_y,\ T_{zz}. \tag{34}$$

(d) For symmetry reasons, $T_{zx}(s_x/2) \equiv 0$ (i.e., for $\alpha = \frac{1}{2}$).

These general characteristics of stress curves have also been observed previously in simulations of 'simple'-fluid films confined between chemically homogeneous but atomically structured (i.e., discrete) substrates [7–10, 13–20]. The substrates were composed of a single layer of Lennard-Jones atoms arranged according to a plane of the face-centred cubic lattice. In the earlier studies the unstrained phase was solidlike on account of a template effect imposed on the confined fluid by the discrete nature of the substrate material. No solidification occurs here under the present thermodynamic conditions.

4.1.2. The impact of substrate corrugation. As far as the present model is concerned, the degree of chemical corrugation of the substrate has significant consequences for the yield-point location $(\alpha^{yd}, T_{zx}^{yd})$. For the subsequent discussion it is convenient to cast chemical corrugation quantitatively in terms of the ratio $c_r := d_s/s_x$. Plots of stress curves for various values of c_r are shown in figure 4(a). For monolayer bridge phases and fixed $s_x = 10$, one can see from figure 4(a) that both T_{zx}^{yd} and α^{yd} are smallest for the smallest $c_r = \frac{2}{10}$. For $c_r < \frac{2}{10}$ only gas phases are thermodynamically stable because the strongly attractive portion of the substrate is too small to support formation of denser (bridge) phases. As c_r increases, both T_{zx}^{yd} and α^{yd} increase until they reach their maximum values $(\alpha^{yd} s_x, T_{zx}^{yd}) \approx (2.740, 0.169)$ for

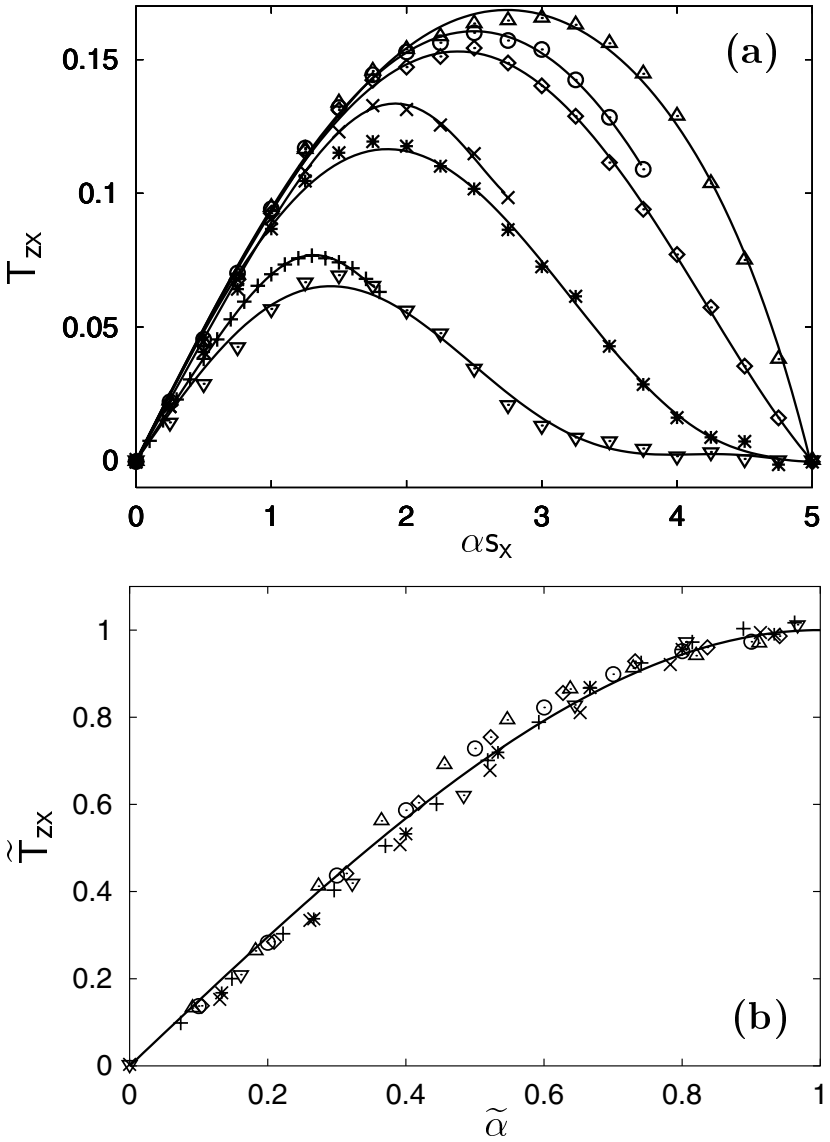

Figure 4. (a) Stress curves $T_{zx}(\alpha s_x)$ for various chemical corrugations $c_r = \frac{2}{10}$ (+), $\frac{3}{10}$ (×), $\frac{4}{10}$ (○), $\frac{5}{10}$ (△), $\frac{6}{10}$ (◇), $\frac{7}{10}$ (∗), $\frac{8}{10}$ (▽). Solid lines are intended to guide the eye. (b) A reduced stress curve $\widetilde{T}_{zx}(\widetilde{\alpha})$ (see (39)) where the symbols are referring to data plotted in (a). The solid line is a representation of (40).

$c_r = \frac{5}{10}$. For larger $c_r > \frac{5}{10}$, the plots in figure 4(a) show that both T_{zx}^{yd} and α^{yd} decrease again until $(\alpha^{yd}s_x, T_{zx}^{yd}) \approx (1.550, 0.069)$ for $c_r = \frac{8}{10}$, which is the largest substrate corrugation for which bridge phases were observed. For $c_r > \frac{8}{10}$, only thermodynamically stable liquid phases formed in the simulations, incapable of sustaining a shear strain.

One also notices from figure 4(a) that stress curves for $c_r = \frac{2}{10}$, $\frac{3}{10}$, and $\frac{4}{10}$ apparently do not cover the entire range of shear strains. In these cases the strongly attractive portion of the substrates is too narrow to stabilize the denser portion of a bridge phase regardless of the

applied shear strain. At some strain threshold $\alpha^{\mathrm{c}} s_x$, the bridge phase is simply 'torn apart' and undergoes a first-order phase transition to a gaslike phase. This gaslike phase, by virtue of its microscopic structure (see figure 2(c)), is incapable of sustaining a shear stress. Thus, at $\alpha^{\mathrm{c}} s_x$, T_{zx} drops to zero discontinuously such that $T_{zx} \equiv 0$ for all $\{\alpha | \alpha^{\mathrm{c}} \leqslant \alpha \leqslant \frac{1}{2}\}$. For the sake of clarity we do not plot this part of the stress curves in figure 4(a). We will report on this (and other) shear-strain-induced phase transitions in a separate publication [35].

Despite this nonmonotonic variation of the yield-point location with c_{r}, it turns out that within the theory of corresponding states [38] it is feasible to renormalize stress curves such that all data points fall onto a unique master curve. Renormalization is effected by introducing dimensionless variables $\widetilde{T}_{zx} := T_{zx}(\widetilde{\alpha} s_x; c_{\mathrm{r}}) / T_{zx}^{\mathrm{yd}}(c_{\mathrm{r}})$ and $\widetilde{\alpha} := \alpha s_x / \alpha^{\mathrm{yd}}(c_{\mathrm{r}}) s_x$. Normalization by α^{yd} and T_{zx}^{yd} is consistent with the theory of corresponding states because it was pointed out in [14] that the yield point may be perceived as a shear critical point analogous to the liquid–gas critical point in pure homogeneous fluids. If the simulation data plotted in figure 4(a) are renormalized according to this recipe, they can indeed be represented by a master curve as the plot in figure 4(b) shows.

4.1.3. Universality of stress curves. The remarkable insensitivity of $\widetilde{T}_{zx}(\widetilde{\alpha})$ to variations of c_{r} can be rationalized as follows. Because of the Hookean regime in the limit $\alpha s_x \to 0$, c_{44} should be approximately constant and positive in this limit. A typical plot in figure 5 confirms this notion. However, because of (34) one expects c_{44} to decline from its Hookean value as $\alpha s_x \to \alpha^{\mathrm{yd}} s_x$, also in agreement with figure 5. Furthermore, since figure 5 shows that the variation of c_{44} with αs_x is not too strong over the range $\{\alpha | 0 \leqslant \alpha \leqslant \alpha^{\mathrm{yd}}\}$, it seems sensible to expand c_{44} in a power series according to

$$c_{44}(\alpha s_x) = \sum_{k=0}^{\infty} \frac{1}{k!} \frac{\mathrm{d}^{(k)} c_{44}}{\mathrm{d}(\alpha s_x)^k}\bigg|_{\alpha=0} (\alpha s_x)^k = \sum_{k=0}^{\infty} a_k (\alpha s_x)^k \simeq a_0 + a_2 (\alpha s_x)^2 \qquad (35)$$

where we refer to the far right side as the small-strain approximation. Notice that the set of coefficients $\{a_k\}$ refer to the *unstrained* bridge phase (i.e., $\alpha = 0$). A molecular expression

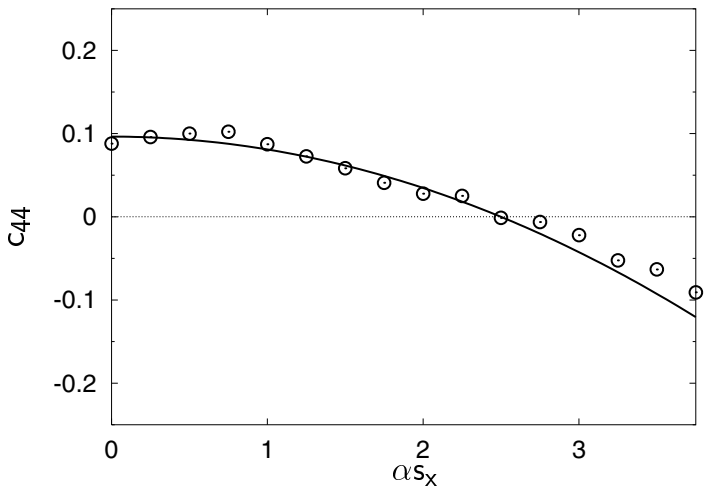

Figure 5. Shear modulus c_{44} as a function of shear strain αs_x. ○: Monte Carlo simulations in the grand mixed stress–strain ensemble; ——: representation of the small-strain approximation $c_{44}(\alpha s_x) = a_0 + a_2 (\alpha s_x)^2$ (see (35), (36)).

for $a_0 \equiv c_{44}(0)$ is given in (30). In the small-strain approximation, a_2 accounts for deviations from Hookean behaviour and may therefore be interpreted as a measure of the plasticity of the unsheared confined film. From symmetry considerations detailed in section 2 and section 3.2 and the definition of $\{a_k\}$ in (35), it is furthermore clear that for $\alpha = 0$, $a_{2k-1} \equiv 0$ ($k = 1, \ldots, \infty$). However, we note in passing that these coefficients do not vanish *a priori* for $\alpha \neq 0$ for symmetry reasons (see section 3.2). From (29) and (35) we obtain the (shear stress) equation of state

$$T_{zx}(\alpha s_x) = \int_0^{\alpha s_x} \mathrm{d}(\alpha' s_x)\, c_{44}(\alpha' s_x) \simeq a_0 \alpha s_x + \frac{1}{3} a_2 (\alpha s_x)^3 \tag{36}$$

based upon the small-strain approximation. In principle, a_0 and a_2 are determined by the ordinate and initial curvature of the function $c_{44}(\alpha s_x)$ ($\alpha \to 0$) (see figure 5). The latter is extremely difficult to extract given the typical accuracy with which the shear modulus can be calculated in our Monte Carlo simulations (see figure 5). However, an accurate estimate is possible based upon (33) which, together with (36), leads to

$$a_0 \equiv c_{44}(0) = \frac{3}{2} \frac{T_{zx}^{\mathrm{yd}}}{\alpha^{\mathrm{yd}} s_x} \tag{37}$$

and

$$a_2 \equiv \frac{1}{2} \frac{\mathrm{d}^2 c_{44}(\alpha s_x)}{\mathrm{d}(\alpha s_x)^2}\bigg|_{\alpha=0} = -\frac{3}{2} \frac{T_{zx}^{\mathrm{yd}}}{(\alpha^{\mathrm{yd}} s_x)^3} \tag{38}$$

in terms of yield stress and strain. These latter quantities can be determined with high precision from (17), (24), and plots similar to the ones shown in figure 3, figure 4(a), and figure 6(a). The validity of (37) is illustrated by table 2 where we compare it with the shear modulus obtained directly from the molecular expression (30) for a selection of unsheared bridge phases. Inserting now (37) and (38) into the equation of state (36) (in the small-strain approximation) together with making the transformations

$$\begin{aligned} \alpha s_x &\to \widetilde{\alpha} := \frac{\alpha s_x}{\alpha^{\mathrm{yd}} s_x} \\ T_{zx} &\to \widetilde{T}_{zx} := \frac{T_{zx}}{T_{zx}^{\mathrm{yd}}} \end{aligned} \tag{39}$$

permits one to recast (36) as

$$\widetilde{T}_{zx} = \frac{\widetilde{\alpha}(3 - \widetilde{\alpha})}{2} \tag{40}$$

Table 2. Comparison of the shear modulus c_{44} from the molecular expression and the yield-point location.

				From (37)	From (30)
c_{r}	$\langle s_z \rangle$	$\alpha^{\mathrm{yd}} s_x$	T_{zx}^{yd}	$c_{44}(0)$	$c_{44}(0)$
$\frac{2}{10}$	2.113	1.350	0.075	0.084	0.079
$\frac{4}{10}$	2.075	2.499	0.161	0.096	0.088
$\frac{4}{10}$	3.057	2.588	0.101	0.058	0.060
$\frac{5}{10}$	2.069	2.743	0.169	0.092	0.101
$\frac{6}{10}$	3.044	2.412	0.095	0.059	0.066

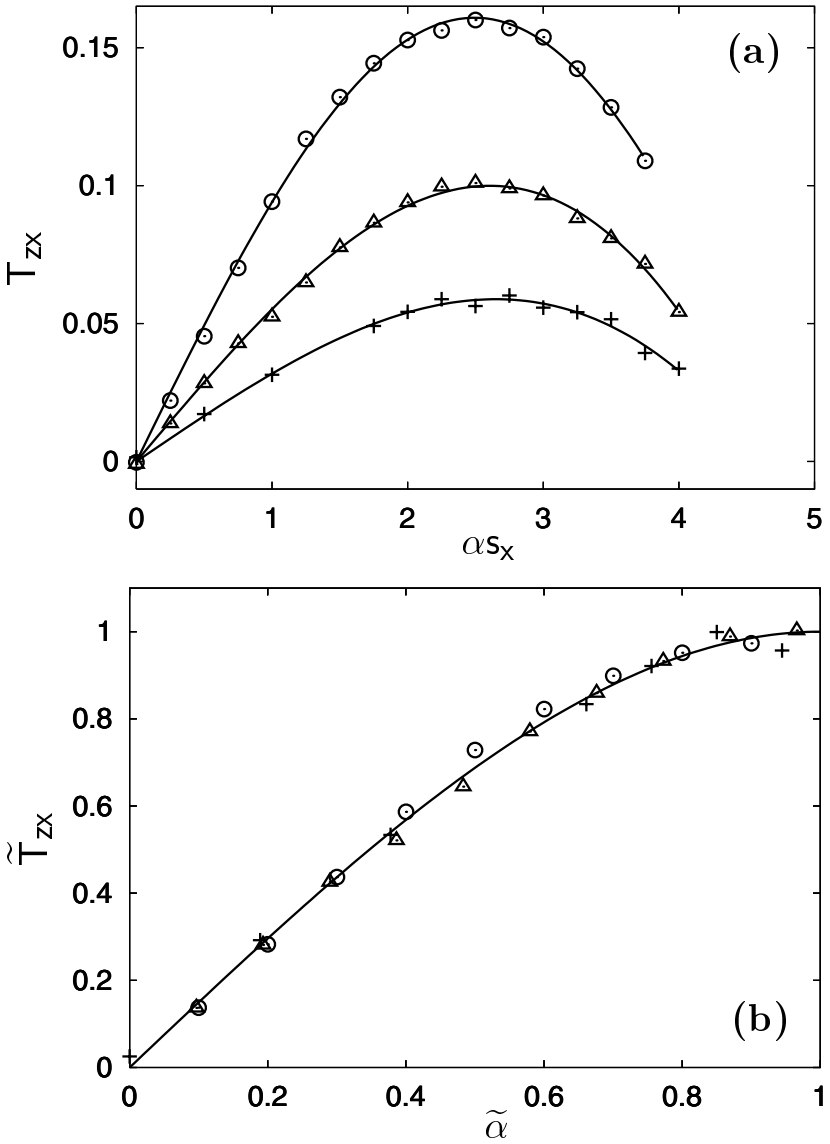

Figure 6. (a) As figure 4(a), but for monolayer (○), bilayer (△), and trilayer (+) morphologies and $c_r = \frac{4}{10}$. (b) As figure 4(b), but for the data points plotted in (a).

where up to the yield point $\{\widetilde{\alpha}|0.0 \leqslant \widetilde{\alpha} \leqslant 1\}$ and $\{\widetilde{T}_{zx}|0 \leqslant \widetilde{T}_{zx} \leqslant 1\}$ are dimensionless numbers, so (40) may be viewed as a master (stress) equation in agreement with the plot in figure 4(b). We emphasize that the master equation is a direct consequence of the small-strain approximation. A unique representation of stress curves is precluded if, on the other hand, one includes higher-order terms proportional to a_{2k} ($k \geqslant 2$) in the expansion (35), because then expressions for $\alpha^{\mathrm{yd}} s_x$ and T_{zx}^{yd} (determined via (34), (36)) depend on the expansion coefficients in a complex way. Thus, if these expressions are introduced in (39) and the resulting equations for T_{zx} and αs_{sx} are inserted subsequently into (36), there is no hope of obtaining a unique expression like (40) free of any material constants $\{a_{2k}\}$ (see also section 5).

It is furthermore noteworthy that universality of stress curves, as defined here, is not restricted to monolayer fluids. Plots of $\widetilde{T}_{zx}$ versus $\widetilde{\alpha}$ in figure 6(b) show that simulation data for monolayer, bilayer, and trilayer bridge phases can also be mapped onto the master curve (40) according to the treatment detailed in this section. Again, the stress curves in figure 6(a) end at some $\alpha^{c}s_x$ because the bridge phases evaporate (see section 4.1.2).

4.2. Thermodynamic stability

From a fundamental point of view, bridge phases comprising different numbers of molecular strata may be viewed as different thermodynamic phases. This interpretation is evident from (10) and (11) indicating that these different bridge-phase morphologies, generally corresponding to different values of s_z and T_{yy}, will exhibit different values of the generalized Gibbs potential $\widehat{\mathcal{G}}$. A multiplicity of morphologies exist despite the fact that the thermodynamic state is uniquely specified by the set $\{T, \mu, s_x, s_y, T_{zz}, \alpha s_x\}$ of natural variables of $\widehat{\mathcal{G}}$. However, from an equilibrium perspective, only the morphology corresponding to the *global* minimum of $\widehat{\mathcal{G}}$ is a thermodynamically stable phase; the others must be metastable.

Fortunately, only a small, finite number of possible morphologies can exist under the present thermodynamic constraints. This can be understood by considering the (normal) compressional stress T_{zz} plotted as a function of substrate separation s_z in figure 7(a). Data plotted in figure 7 were obtained in Monte Carlo simulations in the grand canonical ensemble in which a thermodynamic state is specified by a choice of natural variables similar to the ones determining $\widehat{\mathcal{G}}$, replacing, however, T_{zz} by its conjugate variable s_z. The plot in figure 7(a) shows that T_{zz} is a damped oscillatory function of s_z. These oscillations are fingerprints of stratification—that is, the formation of new fluid layers as the substrate separation increases at constant T and μ [26]. Damping can be ascribed to the decreasing influence of Φ which

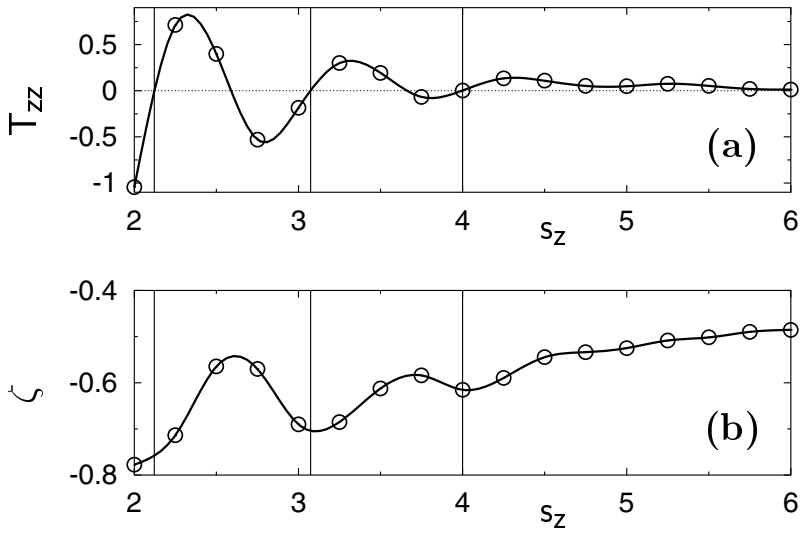

Figure 7. (a) Normal compressional stress T_{zz} (a) (see section III.A in [26] for molecular expressions) as a function of substrate separation from Monte Carlo simulations in the grand canonical ensemble (○) ($\alpha s_x = 0.0$). Solid lines are intended to guide the eye. (b) As (a), but for areal free-energy density ζ (see (10)). Intersections between the latter and vertical lines demarcate (meta- or thermodynamically) stable states in the grand mixed stress–strain ensemble for $T_{zz} = 0.0$ (see the text).

becomes negligible if s_z exceeds some critical value s_z^c. For $\{s_z | s_z \geqslant s_z^c\}$ one expects a homogeneous region to exist in the confined fluid. The homogeneous region is centred halfway between the two substrates, it increases in size with s_z, and its local density (which is independent of position) equals that of a corresponding bulk phase for the same T and μ. As a result, $\lim_{s_z \to \infty} T_{zz}(s_z) = -P_{\text{bulk}}$ where $P_{\text{bulk}}(\mu, T) \simeq 0.03$ is the bulk pressure. In other words, because stratification diminishes with increasing s_z, oscillations in $T_{zz}(s_z)$ vanish eventually, too [39]. Therefore, the plot in figure 7(a) shows that under the present conditions and for $s_z \geqslant 6.0$, stratification becomes subdominant.

In the grand mixed stress–strain ensemble, morphologies consistent with the set $\{T, \mu, s_x, s_y, T_{zz}, \alpha s_x\}$ of state variables can now be identified with intersections between the oscillatory curve $T_{zz}(s_z)$ and the isobar $T_{zz} = \text{constant} \leqslant 0$. However, only intersections for which $\mathrm{d}T_{zz}/\mathrm{d}s_z \geqslant 0$ correspond to (thermodynamically or meta-) stable states as pointed out in [40]; intersections for which $\mathrm{d}T_{zz}/\mathrm{d}s_z < 0$ pertain to unstable states which cannot be realized in Monte Carlo simulations in the grand mixed stress–strain ensemble. The thermodynamically stable morphology corresponds to the intersection having the smallest ζ ($T_{zz} = 0$) according to (10) and (11). With this rationale, an inspection of figure 7 shows that the thermodynamically stable, unstrained morphology ($\alpha = 0.0$) is a monolayer film with $s_z \simeq 2.1$ ($T_{zz} = 0.0$). If confined films are progressively sheared, a parallel analysis of plots in figure 8 and figure 9 shows that the minimum of ζ for $s_z \simeq 2.1$ becomes shallower while another minimum around $s_z \simeq 3.1$, corresponding to a bilayer film, becomes deeper with increasing shear strain. Eventually the depth of the latter minimum exceeds that pertaining to the monolayer film with the result that a bilayer film becomes the thermodynamically stable morphology. Thus, a shear strain exists such that ζ is the same for monolayer and bilayer films. At this shear strain ($A = \text{constant}$), the two morphologies may therefore be viewed as coexisting phases in the usual sense.

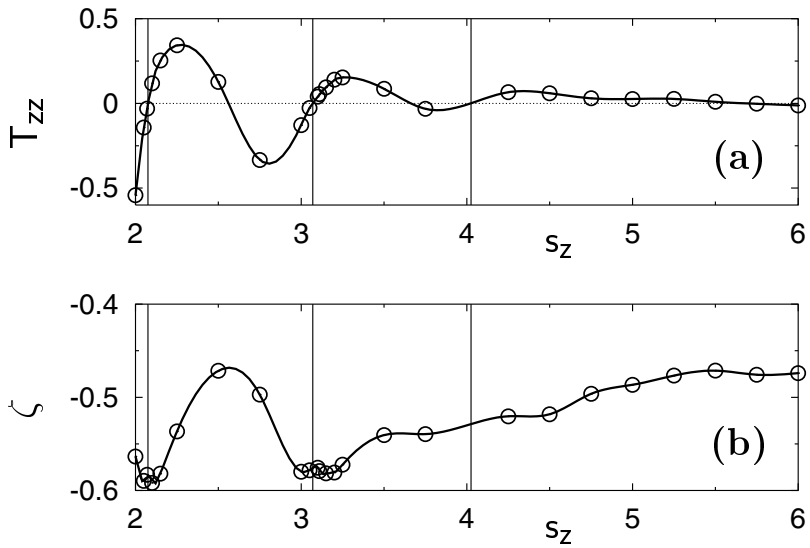

Figure 8. As figure 7, but for $\alpha s_x = 2.25$.

To obtain a more concise picture of thermodynamic stability of different film morphologies, we plot ζ as a function of αs_x in figure 10 for the same system as was analysed in figure 7–figure 9. In a sequence of Monte Carlo simulations in the grand mixed stress–strain

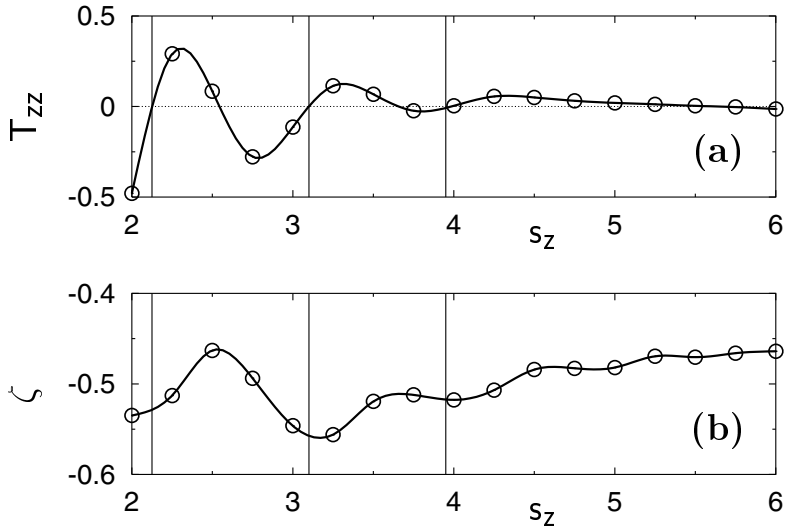

Figure 9. As figure 7, but for $\alpha s_x = 2.50$.

ensemble, we calculate ζ directly from (10) ($T_{zz} = 0$) using the molecular expression for T_{yy} given in (28). An alternative expression for $\zeta(\alpha s_x)$ can be obtained by integrating (9):

$$\zeta(\alpha s_x) = \zeta(0) + \int_0^{\alpha s_x} \mathrm{d}(\alpha' s_x)\; T_{zx}(\alpha' s_x) \qquad \text{fixed } T, \mu, s_x, s_y, T_{zz}$$
$$\simeq \zeta(0) + \frac{a_0}{2}(\alpha s_x)^2 + \frac{a_2}{12}(\alpha s_x)^4 \tag{41}$$

where the second line is based upon the small-strain approximation (see (36)). Full lines in figure 10 are representations of (41) where the constants a_0 and a_2 were determined as in section 4.1.3. Solid lines plotted in figure 10(a) are therefore obtained without further adjusting a_0 and a_2; $\zeta(0)$ is taken from Monte Carlo simulations for unstrained bridge phases. The excellent agreement between $\zeta(\alpha s_x)$ from the Monte Carlo simulations in the grand mixed stress–strain ensemble and the small-strain approximation in (41) highlights once more the validity of the latter for all $\{\alpha|\alpha \leqslant \alpha^{\mathrm{yd}}\}$. However, the plot in figure 10(a) also shows that the small-strain assumption is doomed to fail for sufficiently large shear strains in accord with one's expectation.

From the plots in figure 10(a) one also notices that ζ (and therefore $\widehat{\mathcal{G}}$, A = constant) is lowest for a monolayer bridge phase over the range $0.0 \leqslant \alpha s_x \lesssim 2.2$ indicating that the monolayer is the thermodynamically stable morphology in this regime. Figure 10(a) also shows that intersections $\alpha^* s_x$ exist at which $\widehat{\mathcal{G}}$ assumes the same value for a pair of different morphologies. Thus, at $\alpha = \alpha^*$ these different morphologies coexist, so the points $\alpha = \alpha^*$ correspond to first-order phase transitions between bridge phases comprising different numbers of molecular strata. While there is no obvious relationship between α^* for the coexistence of monolayer and bilayer morphologies and α^{yd}, we notice that for all the cases investigated a monolayer film is the thermodynamically stable morphology for all $\{\alpha|\alpha \leqslant \alpha^{\mathrm{yd}}\}$, so up to the yield point, the plots in figure 4 apparently pertain to thermodynamically stable phases.

Thicker films are therefore thermodynamically stable only if the shear strain exceeds the yield strain. For example, plots in figure 10(b) for $c_{\mathrm{r}} = \frac{6}{10}$ show that ζ for a bilayer bridge phase is lower than for the corresponding monolayer bridge phase over the range $2.3 \lesssim \alpha s_x \leqslant 5.0$ where the bilayer bridge phase is the thermodynamically stable phase according to the above

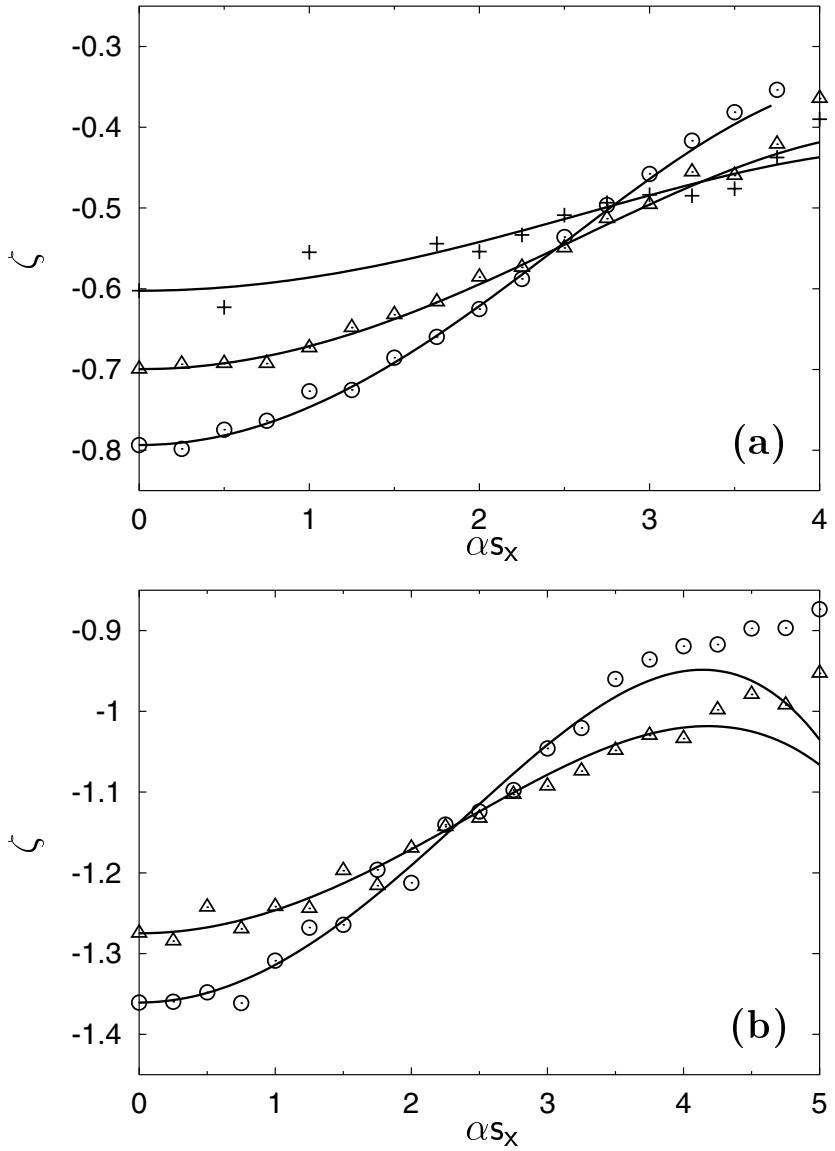

Figure 10. (a) Areal free-energy density ζ as a function of shear strain αs_x for monolayer (○), bilayer (△), and trilayer (+) morphologies calculated in grand mixed stress–strain ensemble Monte Carlo simulations (see (10), (28)) for $c_r = \frac{4}{10}$. The solid lines are calculated from (41). (b) As (a), but for $c_r = \frac{6}{10}$.

discussion. An additional trilayer bridge phase was investigated for $c_r = \frac{4}{10}$, as plots in figure 10(a) show. For $c_r = \frac{4}{10}$, the bilayer is thermodynamically stable over the range $2.4 \lesssim \alpha s_x \lesssim 3.3$ whereas the trilayer film seems to be thermodynamically stable over the range $3.3 \lesssim \alpha s_x \lesssim 4.0$ where all three curves end. However, for the trilayer morphology the statistical error of $\zeta(\alpha s_x)$ is already quite large because T_{yy} is small (see figure 7–figure 9). For $\alpha \simeq 4.0$, bridge phases become unstable and the system undergoes a first-order phase transition to a gas phase [34, 35].

5. Discussion and conclusions

In this paper we investigate the behaviour of fluids confined between plane-parallel, chemically patterned substrates consisting of alternating weakly and strongly adsorbing solid slabs. Under favourable thermodynamic conditions a higher-density portion of the confined fluid stabilized by the strongly adsorbing substrate material is surrounded by a lower-density portion supported by its weakly adsorbing parts. We refer to this structure as a bridge phase. By misaligning the substrates along the x-direction, bridge phases can be exposed to a shear strain and the associated shear stress can be calculated from molecular expressions. We employ a grand mixed stress–strain ensemble in which the film is open to a thermal, material, and normal-stress reservoir to mimic to some extent conditions characteristic of parallel experiments employing the SFA. These experiments permit one to measure almost routinely the rheological properties of molecularly thin confined films.

Our findings can be summarized as follows:

(a) Most importantly, confined phases can have a noncrystalline structure and yet are able to sustain a nonvanishing shear strain. This implies that mere confinement, which, in the present model, reduces molecular mobility in one direction, is sufficient to account for the rheological behaviour of confined phases (see figure 3, figure 4, figure 6).
(b) Stress curves for strained bridge phases are qualitatively similar to those obtained earlier for strained solidlike confined films in that they exhibit a Hookean regime for small strains and a yield point on account of an increasingly plastic response at higher shear strains (see figure 3(a), figure 6(a) and figure 11(a)).
(c) The shear strain sustained by a bridge phase is typically one order of magnitude smaller compared with earlier results for solidlike films on account of the much higher degree of disorder typical of a bridge phase.
(d) Both yield strain and yield stress depend sensitively and nonmonotonically on the degree of chemical corrugation of the substrate—that is, on the ratio of the widths of the strongly and weakly adsorbing portions of the substrate (see figure 4(a)).
(e) Within the framework of the theory of corresponding states [38], different stress curves can be renormalized in terms of yield strain and stress so that all data fall onto a unique master curve for shear strains up to the yield strain (see figure 4(b), figure 6(b)). This supports an earlier interpretation [14] which viewed the yield point as the shear analogue of the liquid–gas critical point in pure homogeneous fluids.

A master equation is obtained upon expanding the shear modulus in terms of the shear strain retaining only terms up to second order. If higher-order terms are included a unique representation of the stress curve is impossible because the resulting analytic expression for the renormalized stress will inevitably depend on properties of the specific bridge phase considered.

The possibility of renormalizing stress curves according to (39) was first noted by Bordarier *et al* [15]. These authors studied 'simple'-fluid films confined between discrete substrates and observed that for different loads T_{zz} and temperatures T, stress curves for films of variable thickness can be mapped onto a unique master curve similar to those in figure 4(b) and figure 6(b) of this work. To interpret their data, Bordarier *et al* employ a fit equivalent to the expansion (35) including, however, terms up to a_4 (see (5) of [15]). However, as pointed out in section 4.1.3, a unique representation of various stress curves is precluded *formally* at the level of the expansion utilized by Bordarier *et al*. It is then not surprising that the parameters required to represent the renormalized stress curves through their fit function show a small dependence on the specific thermodynamic state considered (see table 2 of [15]). However, if truly unique, a consistent representation of various renormalized stress curves by

a master equation must be free of any adjustable parameters like (40) of this work. The (small) inconsistency in the analysis of Bordarier *et al* can also be seen from their figure 4–figure 6 where the representation of their renormalized simulation data by the fit function seems to reach $\widetilde{T}_{zx} = 1$ for $\widetilde{\alpha} < 1$. One is therefore forced to conclude that the demonstration of uniqueness of stress curves in [15] is not entirely convincing. However, in view of this work it seems likely that a universal representation of stress curves presented in [15] would be possible based upon (40). This notion is supported by the plot in figure 11 where we show that even for a film of spherically symmetric Lennard-Jones molecules between discrete substrates (see section 1) the theory of corresponding states (see (40)) can be employed to predict the (normalized) stress curve. However, here the term $T_{zx}A\ \mathrm{d}(\alpha s_x)$ in (9) must be replaced by $T_{zx}A\ \mathrm{d}(\alpha\ell)$ ($0.0 \leqslant \alpha \leqslant 0.5$, $\ell = 2^{2/3}$ for the (perfect) (100) structure of a face-centred cubic lattice at $T = 0$) on account of the discrete atomic structure of the substrate (see section 1). Consequently, the first expression in (39) has to be replaced by its analogue (see figure 11(b))

$$\widetilde{\alpha} := \frac{\alpha\ell}{\alpha^{\mathrm{yd}}\ell}. \tag{42}$$

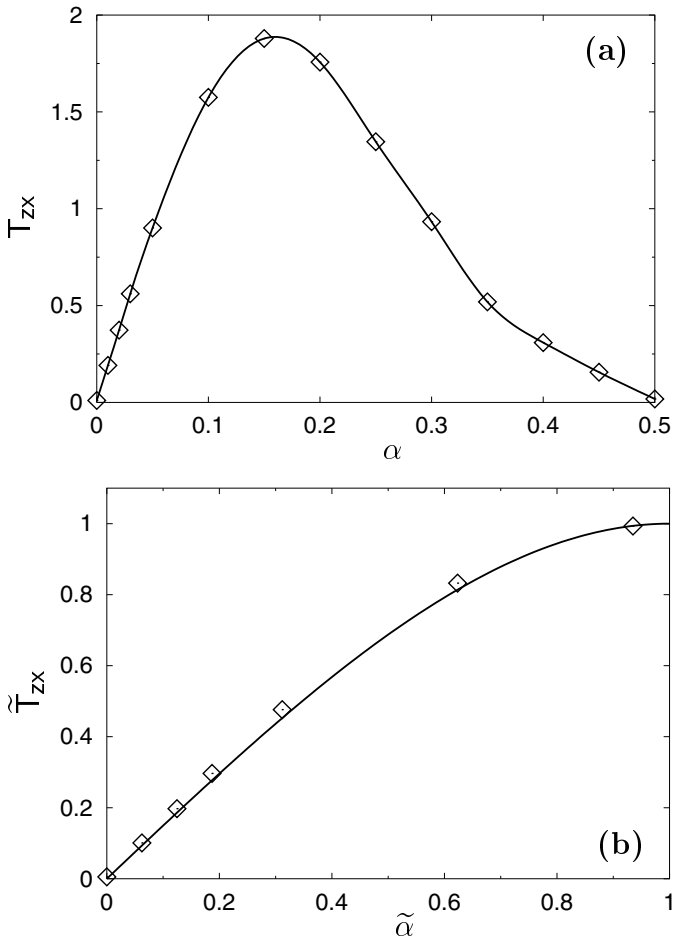

Figure 11. As figure 4, but for a solidlike film forming between discrete substrates (from [13]; see the text).

Furthermore, since the unsheared ($\alpha = 0$) film in figure 11 is solidlike (see figure 2(c) and figure 6 of [13]) and because figure 4(b) shows the validity of the theory of corresponding states even if the confined phase is noncrystalline, it seems highly unlikely that the general response of confined condensed matter to a shear strain (up to the yield point) reflects the presence or absence of solidlike order in any sense. In other words, as far as *confined* phases are concerned our findings do not support the notion that 'the ability to sustain a shear stress is a fundamental signature of a solid: a liquid, by definition, cannot sustain such a stress' (quoted from [3]). On the contrary, the only difference between strained solidlike and fluidic phases in confinement is the *magnitude* of yield stresses and strains, which may well differ by an order of magnitude depending on the degree of order present. This is illustrated by comparing the maxima of the stress curves plotted in figure 3 and figure 11 as well as by noting that for the same value of α the shear strains differ by a factor of $s_x/\ell \simeq 6.3$ between the present model with chemically corrugated substrates and the one with atomically structured substrate surfaces. However, we emphasize that there is no obvious relation between the yield-point location (α^{yd}, T_{zx}^{yd}) and the degree of order. If one wishes to determine whether or not the confined phase is solidlike, an analysis of its microscopic structure in terms of suitably defined spatial correlation functions is absolutely indispensable. It is impossible to determine the physical state of the confined phase solely from its thermomechanical properties.

If solidlike structure is not the sole cause of the rheological behaviour of confined phases, by what more general principle may it be accounted for? Our study suggests that the more likely origin of the response of confined phases to shear deformations is their inhomogeneity in the direction of the applied shear strain induced by the substrate under suitable thermodynamic conditions. An example are the present bridge phases which are characterized by a local density depending on the position in the x-direction (see figure 2(a)). Consequently, if sheared in this direction, a nonvanishing shear stress is obtained. Since, on the other hand, the structure of a bridge phase is translationally invariant in the y-direction, $T_{zy} \equiv 0$. If thermodynamic conditions are such that gas or liquid phases occupy the accessible space between the present substrates, the confined phase is (nearly) homogeneous in both the x- and the y-direction. Consequently, the response of these phases to shear deformation is nullified in accord with the above rationale. Notice that unsheared solidlike phases between discrete substrates are also inhomogeneous but on an atomic length scale, because film molecules vibrate around their equilibrium positions with an amplitude much smaller than ℓ. However, in this case the film is inhomogeneous in both the x- and the y-direction. Hence, a nonzero stress is detected if the confined phase is sheared in the direction of *any* unit vector in the x–y plane.

If inhomogeneity in transverse direction(s) rather than solidification is the cause of the rheology of confined soft condensed matter, it also seems easier to rationalize experimental data for a variety of confined organic substances involving cyclic and chainlike hydrocarbons [3, 4, 22, 41–43]. Regardless of details of molecular structure, the responses of these various fluids to a shear strain are qualitatively the same if they are confined to molecularly small gaps by mica surfaces, say. Given the crystal structure of mica, on the other hand, it seems rather unlikely that all these fluids solidify under confinement conditions. Interestingly, Qiao and Christenson [44] have recently reported on the absence of solidification in confined phases at temperatures above the bulk melting point, thus contradicting the observations of [3,4,42,43]. However, since the confining substrates in the SFA cannot be expected to be perfectly planar on an atomic scale, it seems possible that the confined films are inhomogeneous in directions of the applied shear strain which could account for the observed resistance towards shear deformations according to our above line of arguments. This, in turn, would also imply that most of the simulational work to date (studying solidlike films) deals with a very special situation which may bear only little or no resemblance to situations encountered in SFA experiments.

Acknowledgments

We acknowledge financial support from the Sonderforschungsbereich 448 'Mesoskopisch strukturierte Verbundsysteme'. We also thank the Konrad-Zuse-Institut (Berlin) for a generous allotment of computer time.

References

[1] Harrowell P 1999 *Supramolecular Structures in Confined Geometries* ed G G Warr and S Manne (Oxford: Oxford University Press)
[2] Israelachvili J N 1992 *Intermolecular and Surface Forces* (London: Academic)
[3] Klein J and Kumacheva E 1998 *J. Chem. Phys.* **108** 6996
[4] Kumacheva E and Klein J 1998 *J. Chem. Phys.* **108** 7010
[5] Schoen M 2000 *Computational Methods in Colloid and Interface Science* ed M Borówko (New York: Dekker) at press
[6] Persson B N J 1993 *Phys. Rev.* B **48** 18 140
[7] Thompson P A and Robbins M O 1990 *Science* **250** 792
[8] Thompson P A and Robbins M O 1990 *Phys. Rev.* A **41** 6830
[9] Lupkowski M and van Swol F 1991 *J. Chem. Phys.* **95** 1995
[10] Thompson P A, Grest G S and Robbins M O 1992 *Phys. Rev. Lett.* **68** 3448
[11] Rozman M G, Urbakh M and Klafter J 1996 *Phys. Rev. Lett.* **77** 683
[12] Rozman M G, Urbakh M and Klafter J 1996 *Phys. Rev.* E **54** 6485
[13] Schoen M, Hess S and Diestler D J 1995 *Phys. Rev.* E **52** 2587
[14] Bordarier P, Schoen M and Fuchs A H 1998 *Phys. Rev.* E **57** 1621
[15] Bordarier P, Rousseau B and Fuchs A H 1998 *Thin Solid Films* **330** 21
[16] Schoen M, Rhykerd C L Jr, Diestler D J and Cushman J H 1989 *Science* **245** 1989
[17] Schoen M, Diestler D J and Cushman J H 1993 *Phys. Rev.* B **47** 5603
[18] Diestler D J, Schoen M and Cushman J H 1993 *Science* **262** 545
[19] Schoen M, Diestler D J and Cushman J H 1994 *J. Chem. Phys.* **100** 7707
[20] Schoen M 1996 *Mol. Simul.* **17** 369
[21] Bordarier P 1997 *Les Forces de Surfaces des Systèmes Nanolubrifiés. Simulations et Théorie* (Paris: Université de Paris-Sud Press)
[22] Granick S 1991 *Science* **253** 1374
[23] Allen M P and Tildesley D J 1987 *Computer Simulation of Liquids* (Oxford: Clarendon)
[24] Bock H and Schoen M 1999 *Phys. Rev.* E **59** 4122
[25] Schoen M and Diestler D J 1997 *Chem. Phys. Lett.* **270** 339
[26] Schoen M and Diestler D J 1997 *Phys. Rev.* E **56** 4427
[27] Schoen M 1997 *Physica* A **240** 328
[28] Hill T L 1987 *Statistical Mechanics* (New York: Dover) ch 6
[29] Arfken G 1985 *Mathematical Methods for Physicists* 3rd edn (London: Academic) p 478
[30] Callen H B 1960 *Thermodynamics* (New York: Wiley) ch 13
[31] Schoen M 1999 *Physica* A **270** 353
[32] Schoen M, Diestler D J and Cushman J H 1987 *J. Chem. Phys.* **87** 5464
[33] Wilding N B and Schoen M 1999 *Phys. Rev.* E **60** 1081
[34] Schoen M and Bock H 2000 *J. Phys.: Condens. Matter* at press
[35] Schoen M and Bock H 2000 *J. Phys.: Condens. Matter* at press
[36] Röcken P and Tarazona P 1996 *J. Chem. Phys.* **105** 2034
[37] Röcken P, Somoza A, Tarazona P and Findenegg G H 1998 *J. Phys. Chem.* **108** 8689
[38] Münster A 1969 *Statistical Thermodynamics* vol 1 (Berlin: Springer) ch 8.5
[39] Evans R, Henderson J R, Hoyle D C, Parry A O and Sabeur Z A 1993 *Mol. Phys.* **80** 755
[40] Schoen M, Gruhn T and Diestler D J 1998 *J. Chem. Phys.* **109** 301
[41] Hu H-W, Carson G A and Granick S 1991 *Phys. Rev. Lett.* **66** 2758
[42] Demirel A L and Granick S 1996 *Phys. Rev. Lett.* **77** 2261
[43] Gee M L, McGuiggan P M, Israelachvili J N and Homola A M 1990 *J. Chem. Phys.* **93** 1895
[44] Qiao Y and Christenson H K 1999 *Phys. Rev. Lett.* **83** 1371